Inference and effects of barcode multiplets in droplet-based single-cell assays

Caleb A. Lareau[1,2,3]*, Sai Ma[1,2,4], Fabiana M. Duarte[1,2], Jason D. Buenrostro[1,2]*

[1]Department of Stem Cell and Regenerative Biology, Harvard University, Cambridge, MA 02138, USA

[2]Broad Institute of MIT and Harvard, Cambridge, MA 02142, USA

[3]Division of Medical Sciences, Harvard Medical School, Boston, MA 02115, USA

[4]Department of Biology, Massachusetts Institute of Technology, Cambridge, MA 02142, USA

*Correspondence to: caleblareau@g.harvard.edu or jason_buenrostro@harvard.edu

Abstract

A widespread assumption for single-cell analyses specifies that one cell's nucleic acids are predominantly captured by one oligonucleotide barcode. However, we show that ~13-21% of cell barcodes from the 10x Chromium scATAC-seq assay may have been derived from a droplet with more than one oligonucleotide sequence, which we call "barcode multiplets". We demonstrate that barcode multiplets can be derived from at least two different sources. First, we confirm that ~4% of droplets from the 10x platform may contain multiple beads. Additionally, we find that ~5-7% of beads may contain multiple oligonucleotide barcodes. We show that this artifact can confound single-cell analyses, including the interpretation of clonal diversity and proliferation of intra-tumor lymphocytes. Overall, our work provides a conceptual and computational framework to identify and assess the impacts of barcode multiplets in single-cell data.

Introduction

Droplet-based partitioning systems have become an essential tool for single-cell genomics research. In contrast to plate-based single-cell assays, droplet-based methods, including scRNA-seq[1,2] and scATAC-seq[3,4] enable profiling of thousands of cells in a single experiment. The marked increase in throughput is achieved by parallel barcoding of cellular nucleic acids with beads containing high-diversity DNA barcodes. Critically, downstream computational analyses assume that one barcode sequence equates to one cell.

In this work, we provide multiple lines of evidence that indicate that cells often associate with multiple barcodes by i) multiple beads occurring within the same droplet or ii) heterogeneity of oligonucleotide sequences within a single bead (**Fig. 1a**). Here, we refer to these instances whereby multiple DNA barcodes occur within the same droplet as "barcode multiplets". We find that barcode multiplets can considerably impact single-cell analyses and demonstrate that rare cell events (e.g. the analysis of cell clones) can be particularly affected by this artifact. Further, we provide a computational solution to identify these barcode multiplets in existing single-cell datasets, particularly from the scATAC-seq platform. Finally, we provide recommendations to mitigate these biases in existing assays.

Results

Bead multiplets quantified through imaging

While cell doublet rates are routinely quantified by species-mixing analyses, analogous multiplet rates for bead loading are scarcely discussed. Importantly, commonly used droplet-based assays (e.g. the 10x Chromium platform) leverage a close-packing

ordering of beads[5] to load predominantly one bead per droplet and achieve "sub-Poisson" loading. First, we sought to test this assumption and empirically quantify bead loading within droplets. To achieve this, we loaded hydrogel training beads into droplets following recommended guidelines and imaged the resulting solution. Beads were readily visible and quantifiable per droplet (**Fig. 1b; Fig. S1a-d**), enabling empirical estimates of the number of beads per droplet. A total of 3,865 droplets spanning 30 total fields of view (FOV) over three experimental replicates were quantified (**Table S1**; see **Methods**). Importantly, while the training beads do not differ from those used in the regular protocol, the training buffer is required to visualize beads after loading.

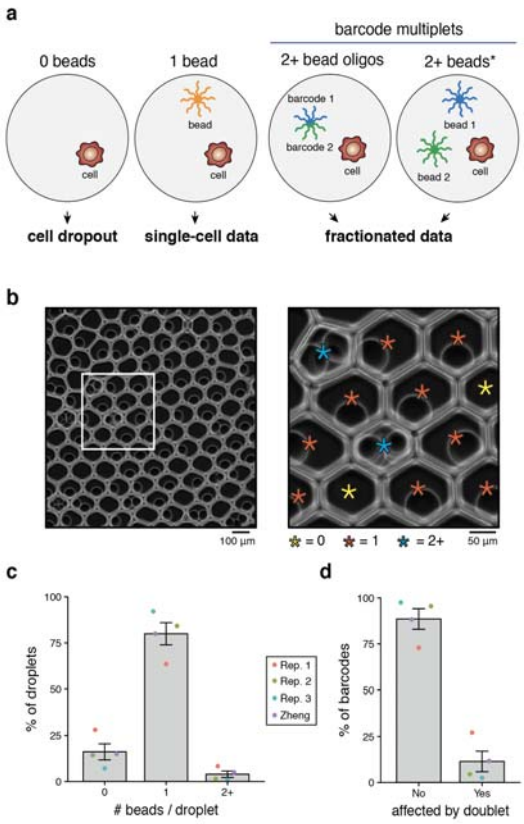

Figure 1 - Quantification of barcode multiplets from multiple beads in 10x Chromium platform. **(a)** Schematic of bead loading variation and phenotypic consequences. Droplets with 0 beads fail to profile nucleic acid from the loaded cell ("dropout") whereas barcode multiplets fractionate the single-cell data. Barcode multiplets can be generated by either heterogeneous barcodes on an individual bead or two or more beads loaded into the same droplet. The * indicates the bead multiplet that can be quantified via imaging. **(b)** Representative example of beads loaded into droplets from the 10x Chromium platform. The white box is magnified 3x for the panel on the right, revealing multiple beads loaded into droplets. Stars indicate beads (except 0) and are colored by the number of beads contained in the droplet. **(c)** Empirical quantification of number of bead barcodes based on image analysis over 3 replicates with previously published data (Zheng *et al.* 2017[2]). **(d)** Percent of barcodes associated with multiplets under the distribution observed in **(c)**. Error bars represent standard error of mean over the experimental replicates.

On average, we found that 16.1% of droplets contained no beads, 80.0% contained exactly one bead, and 3.9% had two or more beads (**Fig. 1c**). These results were consistent with the previously reported results of this platform ("Zheng")[2] and confirm the sub-Poisson loading of beads into droplets (compare to **Fig. S1e** for optimal Poisson loading). While the mean of the bead loading was consistent with previous reports, we note considerable run-to-run variability from our imaging replicates, ranging from 0.8% to 8.4% (**Fig. S1f**). These results indicate that the occurrence of bead multiplets likely varies between machines and individual runs. Furthermore, we noted occurrences of large droplets with multiple beads (**Fig. S1g**) that likely originated from the errant merging of several individual droplets, yielding another source of potential barcode multiplets.

While our estimate of the occurrence of multiple beads in droplets confirms previous reports[2], we emphasize that this problem is exacerbated when considering potential barcodes in single-cell data. On average, we estimate that 11.4% of barcodes would represent barcode multiplets, reflecting droplets with heterogeneous oligonucleotide sequences (**Fig. 1d;** see **Methods**). Moreover, we note that imaging provides a lower-bound estimate for the true occurrence of barcode multiplets for two reasons. First, droplets with four or more beads were assigned a count of four since the exact number of beads could not be reliably determined in these instances (e.g. **Fig. S1d**). Second, imaging cannot evaluate the possibility of heterogeneous beads, a second class of artifact that leads to barcode multiplets (**Fig. 1a**). Despite the alarmingly high prevalence of barcode multiplets, the effect of this confounding phenomenon has not been systematically considered in single-cell analyses. Intuitively, these observed barcode multiplets fractionate data from the cell to multiple barcodes, resulting in a reduction of data per cell and the substantial overestimation of the total number of cells sequenced by artificial synthesis of barcodes reflecting the same single cell. With this artifact could be confirmed by imaging, we sought to further understand its properties and effects in single-cell data.

Identifying barcode multiplets in 10x scATAC-seq data with bap

Recently, we developed a computational framework called bead-based ATAC processing (bap), which identifies instances of barcode multiplets in droplet single-cell ATAC-seq (dscATAC-seq)[3]. Critically, we discriminate between multiple true cells and barcode multiplets by considering the Tn5 insertion sites, noting that barcode multiplets would amplify the same exact fragments (**Fig. 2a; Fig. S2**). Thus, our computational approach leverages the molecular diversity of Tn5 insertion sites across the genome to identify pairs of barcodes that share more insertion sites than expected and merge these corresponding barcode pairs (**Fig. 2a**). Previously, we utilized bap to facilitate

super-loading beads into droplets to achieve a ~95% cell capture rate with a mean 2.5 beads/droplet[3]. Here, we reasoned that bap may identify barcode multiplets in 10x scATAC-seq data.

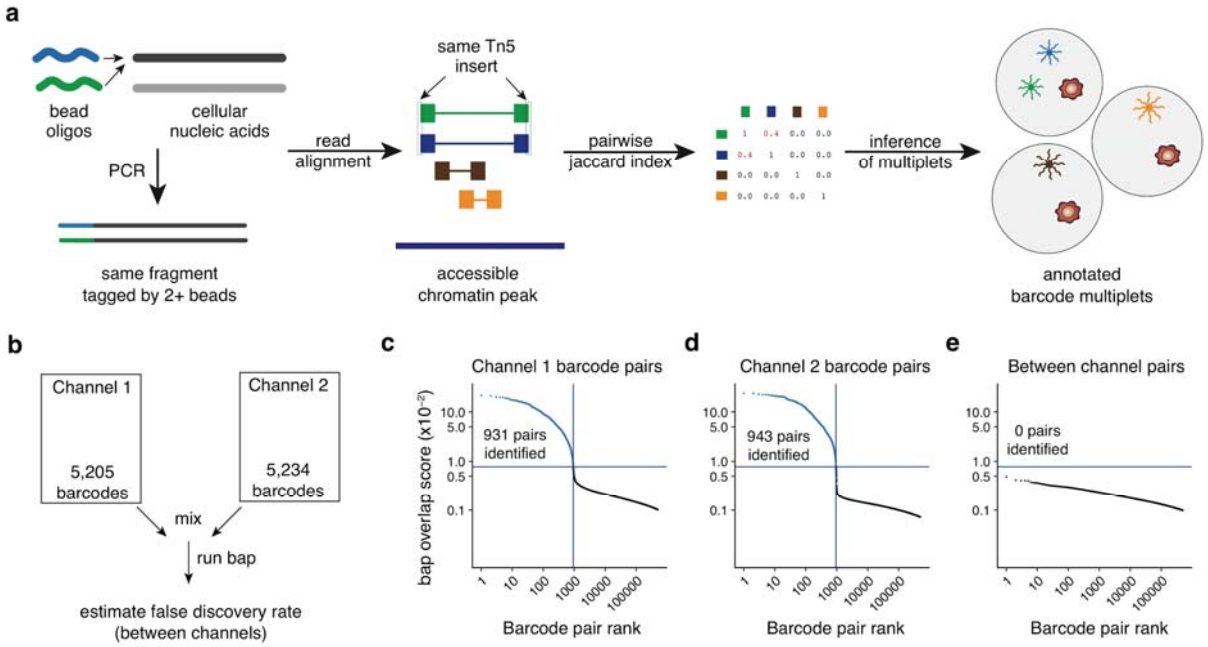

Figure 2 - Verification of bap to identify barcode multiplets using 10x scATAC-seq data. (a) Schematics of methodology to detect barcode multiplets whereby cellular nucleic acids are tagged by two different oligonucleotide sequences and later inferred from sequencing a scATAC-seq library from the same Tn5 insertions per fragment. **(b)** Schematic of mixing experiment. Two channels were combined and the resulting merged files were analyzed with bap. **(c-e)** Knee plots comparing the top 500,000 barcode pairs from **(c)** only channel 1, **(d)** only channel 2, and **(e)** between channels. The number of pairs calls is indicated by the number of points above the blue horizontal line (see **Methods**).

After updating bap to facilitate processing of the 10x scATAC data (**Fig. S2**; see **Methods**), we conducted an initial *in silico* experiment in order to verify the applicability of our approach to 10x scATAC-seq data. Here, we combined two channels from a similar biological source (~5,000 cells of peripheral blood mononuclear cells; PBMCs) and executed bap on the resulting combination (**Fig. 2b**; see **Methods**). As any barcode pairs merged between channels would be false positives, our approach facilitated an estimation of the false positive rate of our approach in 10x data. After executing bap with the default parameters, 1,874 barcode pairs were identified as sharing an unusual number of shared transposition events. Specifically, 931 pairs from channel 1 (**Fig. 2c**) and 943 pairs from channel 2 (**Fig. 2d**) were identified. However, zero pairs were identified between channels (**Fig. 2e**), indiciating a very low false positive rate for bap when applied to this assay. Moreover, the shape of the ranked-ordered barcode pair

curves for the channels separately were distinct from the between-channel curve (**Fig. 2c-e**). Overall, these results support the utility of bap in inferring barcode multiplets from the 10x platform.

After establishing the applicability of bap for 10x scATAC-seq data, we sought to better understand the properties of barcode multiplets determined by bap, focusing on two datasets ("This Study" and "Public"; see **Methods**) of ~5,000 human PBMCs (**Fig. 3a**). Overall, we estimated the percentage of barcodes in multiplets were 13.2% (This Study; **Fig. S3a**) and 17.6% (Public; **Fig. 3b**). These cell barcodes were identified from the high-quality, error-corrected barcode sequences from CellRanger with abundant reads in peaks. Additionally, since individual barcodes in the space of all possible barcodes are separated by a minimum Hamming distance of three in the 10x platform, the high prevalence of barcode multiplets is unlikely to be caused by sequencing errors. Importantly, these implicated barcodes are normally considered in downstream analyses, including cell clustering and clonotype abundance estimates. Furthermore, we suggest that additional multiplets are present in the library but likely did not pass thresholds for reads detected due to the fractionation of data associated with these barcodes (**Fig. S3b**; see **Methods**).

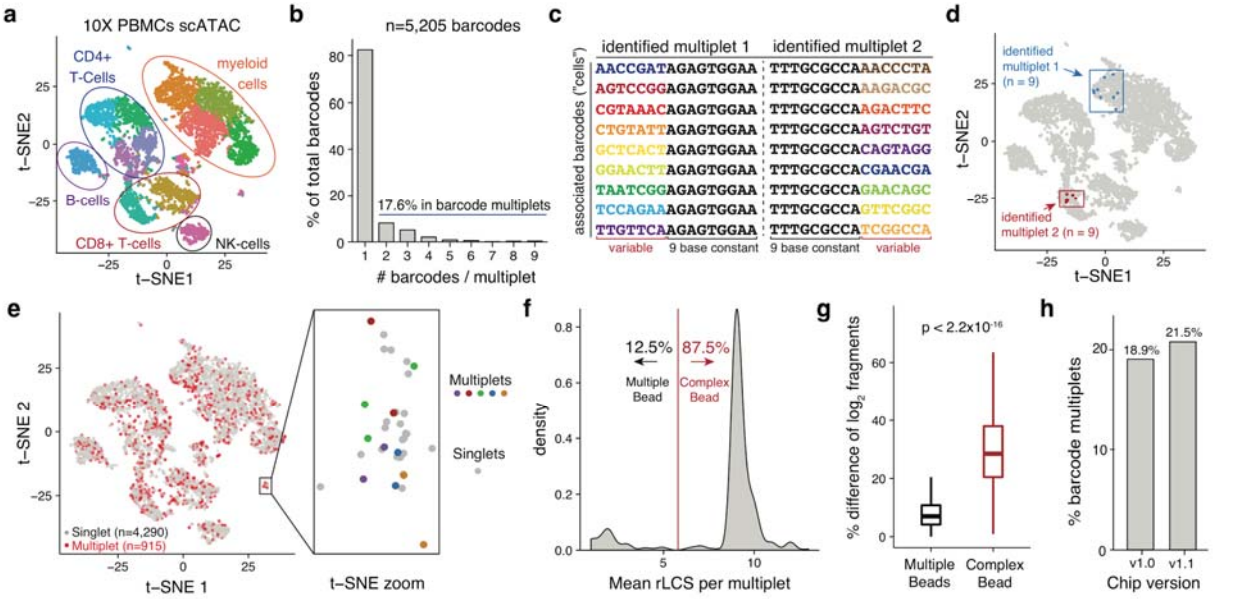

Figure 3 - Inference and effect of barcode multiplets in single-cell ATAC-seq data. (a) Default t-SNE depiction of public scATAC-seq PBMC 5k dataset. Colors represent cluster annotations from the automated CellRanger output. **(b)** Quantification of barcodes affected by barcode multiplets for the same dataset (identified by bap). **(c)** Depiction of two multiplets each composed of 9 oligonucleotide barcodes. Barcodes in each multiplet share a long common subsequence, denoted in black. **(d)** Visualization of two barcode multiplets from **(c)** in t-SNE coordinates. **(e)** Visualization of all implicated barcode multiplets from this dataset. The zoomed panel shows a small group of cells affected by five multiplets, indicated by color. **(f)** Empirical distribution of the mean restricted longest common subsequence (rLCS) per multiplet.

A cutoff of 6 was used to determine either of the two classes of barcode multiplets. **(g)** Percent difference of the mean log2 fragments between pairs of barcodes within a multiplet. The reported p-value is from a two-sided Kolmogorov–Smirnov test. Boxplots: center line, median; box limits, first and third quartiles; whiskers, 1.5x interquartile range. **(h)** Overall rates of barcode multiplets from additional scATAC-seq data comparing v1.0 and v1.1 (NextGEM) chip designs.

Surprisingly, from these experiments, we observed instances in both datasets where barcode multiplets contained at least 7 distinct barcodes (**Table S2; Table S3**). In particular, we observed two instances of multiplets containing 9 unique barcodes in the Public dataset. Here, each implicated barcode contained a restricted longest common subsequence (rLCS) of 9 (**Fig. 3c**; see **Methods**). As such, we suggest that these barcode multiplets likely reflect error during barcode synthesis resulting in a single bead with multiple barcodes, resulting in a “complex bead” (**Fig. 1a**). Visualization of these barcode multiplets from dimensionality reduction using t-distributed stochastic neighbor embedding (t-SNE) confirmed these barcodes reflect markedly similar chromatin accessibility profiles (**Fig. 3d; Fig. S3c**). Overall, barcode multiplets generally co-localized with barcode singlets and do not dramatically alter the interpretation of cell types in an embedding (**Fig. 3e**). However, we find that certain regions of the t-SNE embedding contained a disproportionate concentration of barcode multiplets, which may lead to errant identification of presumed rare cell types (e.g. 5 unique multiplets shown in **Fig. 3e**).

To further elucidate these identified barcode multiplets, we annotated these barcodes with graph-based Louvain clusters (produced using the default CellRanger execution). As expected, we observed a significant enrichment of barcode multiplet pairs occurring in the same cluster (91.1% for This Study; 74.1% for Public) compared to a permuted background (11.6% and 8.6% respectively; **Fig. S3d**; see **Methods**). We note that barcode multiplets not within the same cluster largely reflect barcodes split between multiple clusters of the same cell type (e.g. myeloid cells; see Multiplet 5 in **Fig. S3c** and **Table S3**). Additionally, we observed a statistically-significant association between the Louvain cluster assignment and inferred barcode multiplet status for both This Study (p=0.0065) and Public datasets (p=2.46e-05; chi-squared test; see **Methods**). These results indicate that the barcode multiplets can occur in clusters unevenly, potentially confounding inferences regarding cell-type abundance. Additionally, through iteratively downsampling and re-executing bap, we confirmed the stability of our metric with sequencing depths as low as a median 10,000 fragments detected per barcode (**Fig. S3e**; see **Methods**), confirming the broad utility of this approach. Overall, as these barcode multiplets represent quasi-independent observations of the accessible chromatin landscape of the same single cell, we suggest that these identified barcode multiplets may be utilized in a variety of different useful applications. Examples include

determining sequencing saturation, inferring sequencing biases, and benchmarking bioinformatic clustering approaches. Furthermore, these barcode multiplets can be merged to improve data quality[3].

Contributions of types of barcode multiplets

Having verified the overall detection of the effects of barcode multiplets in these datasets, we sought to determine the relative contributions of each source of barcode multiplets to the overall abundance (**Fig. 1a**). To achieve this, we established a null distribution by computing the rLCS for random pairs of barcodes from the 10x whitelist (see **Methods**). Over 1,000,000 sampled pairs, we determined that pairs with an rLCS ≥6 were extremely uncommon assuming an independent co-occurrence (<0.5% probability of co-occurring; **Fig. S3f**). Thus, for inferred multiplets with a mean rLCS ≥6, we interpret these to be most likely caused by heterogeneous barcodes within a single bead. After computing the mean rLCS between pairs of barcodes per multiplet, we determined that 87.5% of multiplets were likely caused by these complex or heterogeneous beads in the Public dataset (**Fig. 3f**). Using this classification, we could further estimate the prevalence of these complex beads to be 6.9% in this dataset (see **Methods**). Parallel analyses for This Study dataset yielded similar results (83.5% of barcode multiplets were due to complex beads; 4.9% of beads were heterogenous beads). Interestingly, the percent difference between the log2 number of valid fragments for these two classes of multiplets showed greater variability in the number of fragments per barcode for the complex beads than for barcode multiplets presumably caused by two beads (**Fig. 3g;** see **Methods).** This result supports the idea that there may be a predominant individual barcode sequence on these complex beads though there is detectable heterogeneity. Finally, as 10x recently released their v1.1 “NextGem” design, we processed two additional datasets that were run with the two different chip designs in parallel. Our results confirm that the abundance of barcode multiplets persists across both of these two different chip designs (**Fig. 3f**).

Confounding of clonal lymphocytes estimation from barcode multiplets

We suggest that many applications of the 10x Chromium platform are unlikely to be impacted by bead multiplets. However, droplet single-cell approaches are now employed for purposes requiring increasingly precise quantitation, such as highly multiplexed perturbations[6], clonal lymphocyte analyses[7], or diagnostics[8]. Thus, for analyses of rare events, such as those routinely quantified in CRISPR perturbations or in clonal analyses of cells, the surprisingly high prevalence of barcode multiplets may become particularly problematic. As one example, we hypothesized that barcode multiplets may significantly alter quantitation of cell clones distinguished by unique B-

cell receptor (BCR) and T-cell receptor (TCR) sequences in a tumor microenvironment (**Fig. 4a**). Though there is no current approach to define bead multiplets in scRNA-seq data, we reasoned that certain abundant BCR and TCR clonotypes may be explained by complex beads representing one true cell (similar to **Fig. 3c**). To test this, we reanalyzed a publicly available dataset generated using the 10x V(D)J platform that analyzed lymphocytes from a non-small-cell lung carcinoma (NSCLC) tumor (**Fig. 4a**). Indeed, we observed two instances of a BCR clone with four or more cells that could be more parsimoniously interpreted as barcode multiplets derived from a single B-cell (**Fig. 4b**). In particular, all presumed cells from these clones shared an rLCS of ≥9, an extremely unlikely event assuming true clonal cells would be randomly assigned barcode sequences (**Fig. S3f**; **Fig. S4a**). Indeed, the distribution of the rLCS across all BCR clonotypes indicated a detectable bias indicative of barcode multiplets (**Fig. S4a**; see **Methods**). Furthermore, we identified additional clones that were depicted with a more complex heterogeneous structure that still broadly reflected bead synthesis errors (**Fig. 4c**).

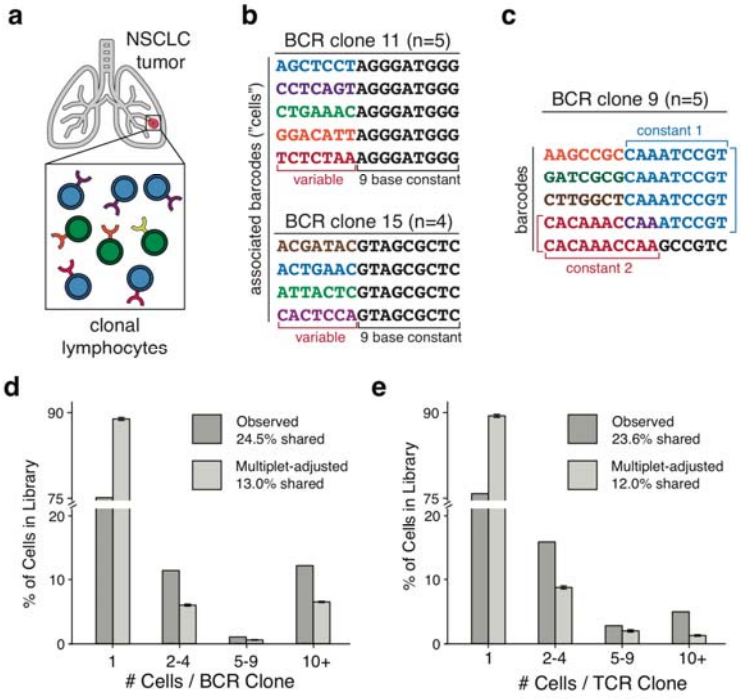

Figure 4 - Confounding of intratumor clonal lymphocytes inference from barcode multiplets. (a) Schematic of intra-tumor lymphocytes identified from single-cell V(D)J sequencing on the 10x platform. **(b)** Identification of two presumed clonotypes composed of 5 and 4 barcodes. These clonotypes are likely to have been derived from one cell observed multiple times via barcode multiplets. **(c)** Example of a presumed clone composed of 5 barcodes with multiple constant sequences. **(d,e)** Overall summary of prevalence of **(d)** B-cell and **(e)** T-cell clone size before and after adjusting for observed rates of barcode multiplets in single-cell data. Error bars represent standard errors of the mean across 100 permutations.

Having established the clear possibility of barcode multiplets occurring in these data, we sought to determine how the interpretation of the overall clonality would be changed when accounting for the barcode multiplets. Using conservative estimates of barcode multiplets from the scATAC-seq analyses, we conducted a series of simulations to determine how the clonality estimates of these lymphoid cells in tumors would become altered after accounting for estimated barcode multiplet levels from bap (see **Methods**). Overall, the percentage of cells associated with a clonotype comprised of at least two cells decreases considerably for both BCR (24.5% to 13.0%; **Fig. 4d**) and TCR (23.6% to 12.0% **Fig. 4e**) clonotypes. Further analyses indicated a clone false discovery rate as high as 50.7% (BCR) and 48.4% (TCR) in these data (see **Methods**), painting a much more conservative picture of clonality within NSCLC tumors, assuming similar rates of barcode multiplets uncovered from bap in the scATAC-seq analyses. The results from these simulations indicate that bead multiplets may significantly confound clonal analysis and that this quantifiable discrepancy may falsely lead to conclusions of clonal expansion of lymphocytes in primary tumors.

Discussion

Overall, our work provides a new perspective to consider barcode multiplets in single-cell data. Though the exact chemistry of the training beads and reaction is different than what is typically employed in the 10x single-cell reactions, our imaging results confirm detectable bead multiplets as previously reported[2]. Additionally, we show that bap, a computational algorithm designed to infer barcode multiplets, can be applied to sequenced scATAC-seq data from the 10x platform and confidently identify barcode multiplets. Further analyses of multiplets identified by bap indicate that putative heterogeneity of beads in the 10x reaction is the predominant driver of the surprisingly high rates of multiplets in these datasets. Moreover, our analyses of clonal cells marked by BCRs and TCRs further suggest that bead sequence heterogeneity may be an artifact present across multiple sources of 10x single-cell data.

As single-cell approaches move toward the precise quantification of rare cell types, trajectories, perturbations, and clones, an understanding of potential artifacts is essential as their confounding effects may become exacerbated in large datasets. Additionally, as these measurements move toward clinical applications[8], particularly in tumors where TCR repertoire may serve as a prognostic biomarker[9], barcode multiplets may significantly confound interpretation. In some analyses (with <15% clones), we anticipate that many identified clonal cells may arise from bead multiplets. While our existing computational approach (bap) can facilitate the identification of barcode multiplets in scATAC-seq data, further experimental and computational tools are needed to more broadly identify these effects in RNA or genome sequencing droplet-

based assays. We envision a combination of dense exogenous barcodes via cell hashing[10] and evolved by CRISPR-Cas9[11] or intrinsic features such as clonal mutations, rearrangements, or highly correlated abundances with barcode sequence similarity metrics could be leveraged to better infer barcode multiplets. Such approaches would complement existing tools that robustly identify cell doublets[12,13] and empty droplets[14] from droplet-based scRNA-seq and further mitigate hidden confounders in single-cell data. Until then, we suggest that inferences regarding rare cell events should be corroborated across multiple channels or technologies to validate interpretation.

Taken together, our estimation and identification of barcode multiplets has a wide range of potential applications and confounding effects that influence widely-used droplet-based single-cell assays.

Supplemental Figures

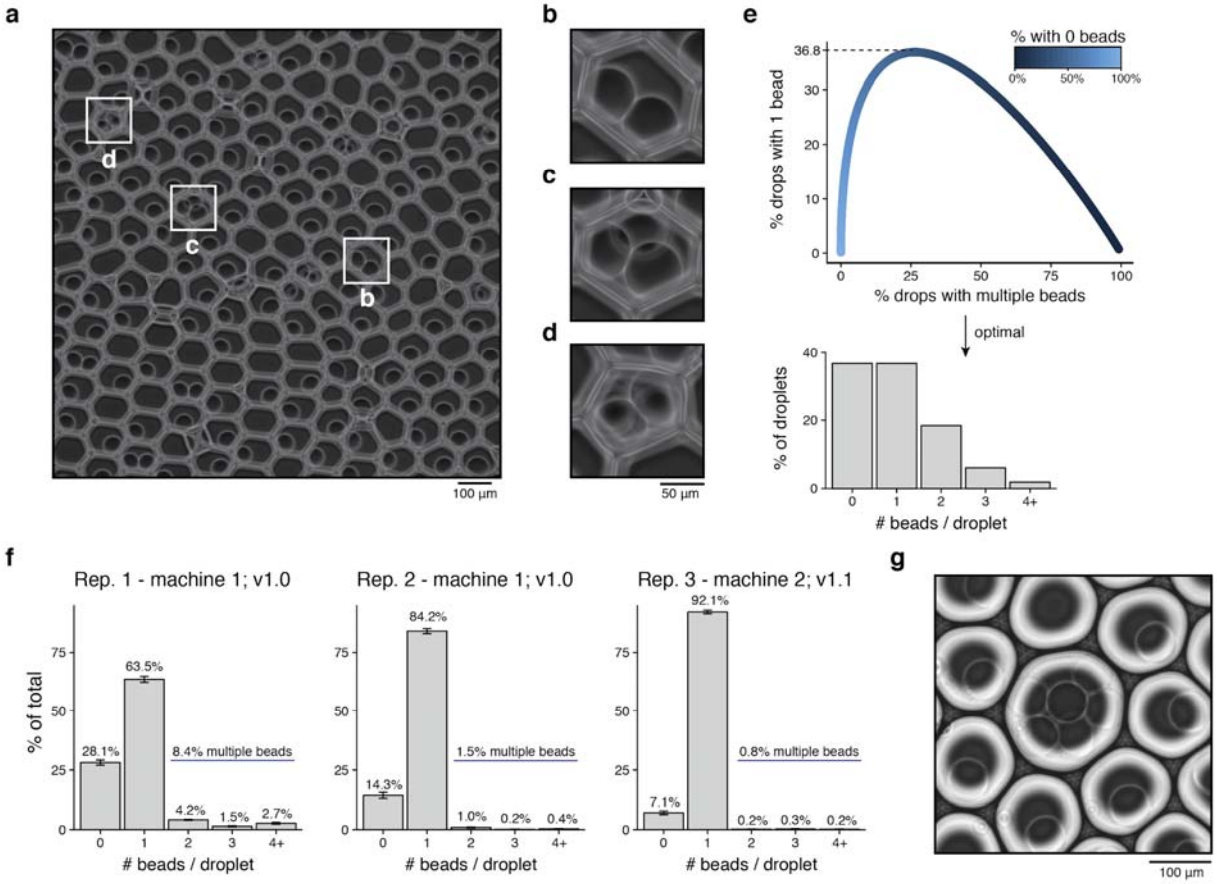

Figure S1 - Supporting information for Figure 1. (a) Alternative field of view. Boxes highlight individual droplets shown in subsequent panels. **(b-d)** Examples of 2, 3, and 4+ beads per droplet, respectively. **(e)** Theoretical support for optimal bead loading under Poisson distribution assumptions. The dotted line (top) represents the theoretical maximum for 1 bead loaded into droplets, and the full distribution at this point is shown in the bar graph. **(f)** Quantification of beads per droplet for each replicate. Above each panel, the machine and the version of the chip used for the training kit is indicated. Error bars represent standard error of mean over 10 fields of view per replicate. **(g)** Example of presumed merged droplet containing multiple (6) beads.

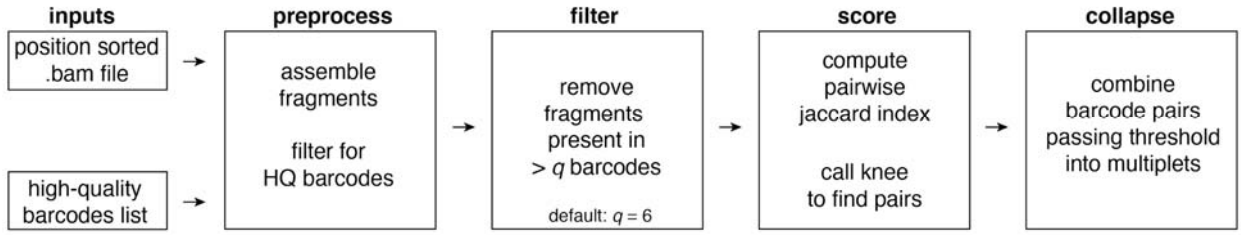

Figure S2 - Supporting information for Figure 2. An overview of the inputs and computational workflow for the application of bap to 10x scATAC-seq data.

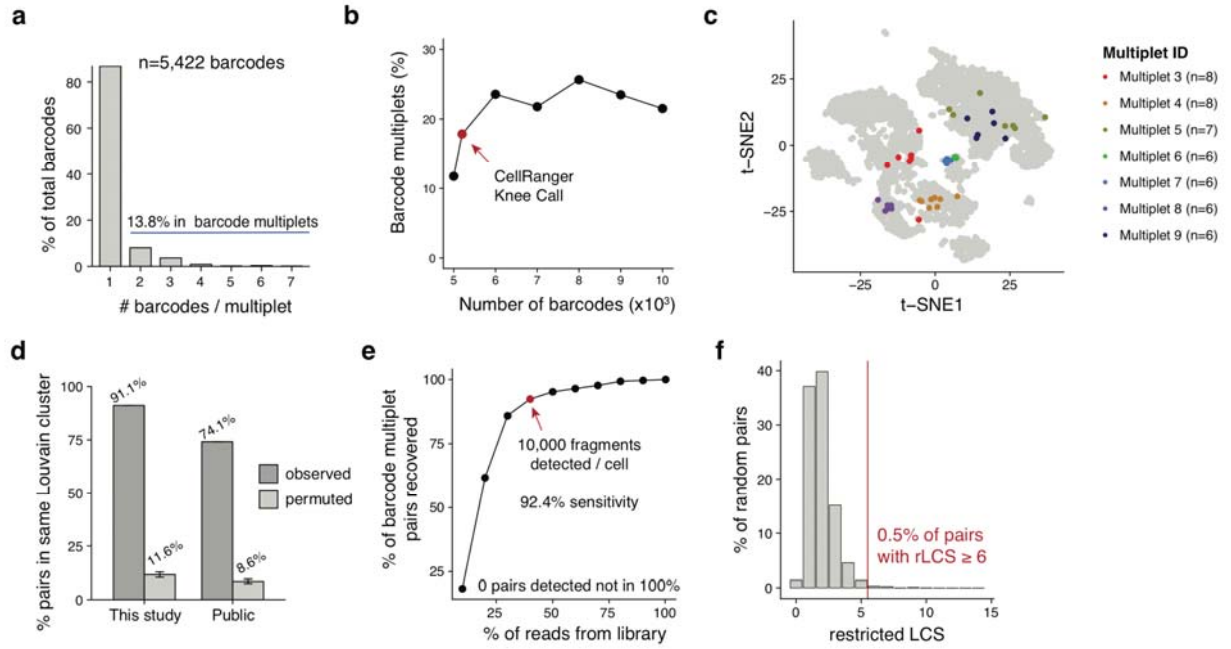

Figure S3 - Supporting information for Figure 3. (a) Quantification of barcodes affected by barcode multiplets for the PBMC dataset generated with this work ("This Study"). **(b)** Percentage of barcode multiplets identified for different numbers of input barcodes (see **Methods**). **(c)** Visualization of seven additional barcode multiplets from the Public dataset. **(d)** Proportion of bead pairs occurring in the same chromatin accessibility-defined Louvain cluster compared to a permuted background. Error bars represent standard error of mean over 100 permutations per dataset. **(e)** Downsampling analysis of the dataset generated in this work ("This Study"). Barcode multiplets were examined at downsampled intervals from 10%-90% by units of 10%. The highlighted sample represents 40% downsampling and corresponds to a median 10,000 fragments detected per barcode. At all downsampled thresholds, we detected 0 pairs that were not present in the 100% sample. **(f)** Distribution of the restricted longest common subsequence (rLCS) for 1,000,000 randomly-sampled barcode pairs in the 10x barcode universe. A threshold at 6 is drawn for use in other analyses.

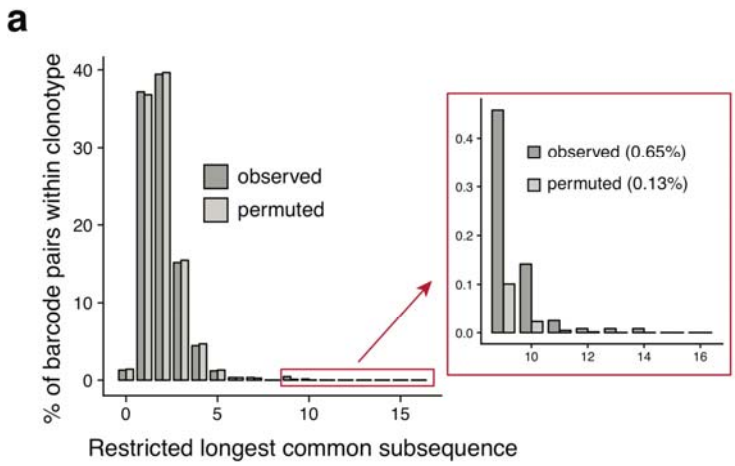

Figure S4 - Supporting information for Figure 4. (a) Overall summary of prevalence of B-cell clone size before and after adjusting for observed rates of barcode multiplets in single-cell data.

Supplemental Tables

Table S1 - Quantifications of bead abundances in droplets across 30 fields of view.

Table S2 - Identified barcode multiplets in 10x Chromium scATAC-seq data.

Table S3 - Highlighted barcode multiplets in Fig. 3d and S3c.

Acknowledgements

We thank J. Ulirsch and members of the Buenrostro lab for insightful comments. We are grateful to A. Labade and L. Ludwig for technical assistance. We thank Z. Burkett and R. Lebowsky of Bio-Rad for helpful conversations. We acknowledge a useful blog post from L. Pachter discussing sub-Poisson bead loading. J.D.B., C.A.L., S.M., and F.M.D. acknowledge support by the Allen Distinguished Investigator Program through the Paul G. Allen Frontiers Group. This work was further supported by the Chan Zuckerberg Initiative. C.A.L. is supported by F31 CA232670 from the NIH.

Author contributions

C.A.L. and J.D.B. conceived and designed the study. C.A.L. implemented the software and performed analyses. S.M. and F.M.D. performed experiments and aided analyses. J.D.B. supervised the work. All authors participated in the writing of the manuscript.

Code and data availability

Software associated with the barcode multiplet identification and merging algorithm is available at https://github.com/caleblareau/bap. Code and data to reproduce the main findings of this study are available at https://github.com/caleblareau/barcode-multiplets. The public 10x scATAC-seq datasets are available for download at https://support.10xgenomics.com/single-cell-atac/datasets and the public NSCLC clonotypes at https://www.10xgenomics.com/solutions/vdj/.

References

1. Klein, A. M. & Macosko, E. InDrops and Drop-seq technologies for single-cell sequencing. *Lab Chip* **17**, 2540–2541 (2017).
2. Zheng, G. X. Y. *et al.* Massively parallel digital transcriptional profiling of single cells. *Nat. Commun.* **8**, 14049 (2017).
3. Lareau, C. A. *et al.* Droplet-based combinatorial indexing for massive-scale single-cell chromatin accessibility. *Nat. Biotechnol.* (2019). doi:10.1038/s41587-019-0147-6
4. Satpathy, A. T., Granja, J. M., Yost, K. E., Qi, Y. & Meschi, F. Massively parallel single-cell chromatin landscapes of human immune cell development and intratumoral T cell exhaustion. *BioRxiv* (2019).
5. Abate, A. R., Chen, C.-H., Agresti, J. J. & Weitz, D. A. Beating Poisson encapsulation statistics using close-packed ordering. *Lab Chip* **9**, 2628–2631 (2009).
6. Dixit, A. *et al.* Perturb-Seq: Dissecting Molecular Circuits with Scalable Single-Cell RNA Profiling of Pooled Genetic Screens. *Cell* **167**, 1853–1866.e17 (2016).
7. Simone, M. D., De Simone, M., Rossetti, G. & Pagani, M. Single Cell T Cell Receptor Sequencing: Techniques and Future Challenges. *Frontiers in Immunology* **9**, (2018).
8. Haque, A., Engel, J., Teichmann, S. A. & Lönnberg, T. A practical guide to single-cell RNA-sequencing for biomedical research and clinical applications. *Genome Med.* **9**, 75 (2017).
9. Cui, J.-H. *et al.* TCR Repertoire as a Novel Indicator for Immune Monitoring and Prognosis Assessment of Patients With Cervical Cancer. *Front. Immunol.* **9**, 2729 (2018).
10. Stoeckius, M. *et al.* Cell Hashing with barcoded antibodies enables multiplexing and doublet detection for single cell genomics. *Genome Biol.* **19**, 224 (2018).
11. Raj, B. *et al.* Simultaneous single-cell profiling of lineages and cell types in the vertebrate brain. *Nat. Biotechnol.* **36**, 442–450 (2018).
12. Wolock, S. L., Lopez, R. & Klein, A. M. Scrublet: Computational Identification of Cell Doublets in Single-Cell Transcriptomic Data. *Cell Syst* **8**, 281–291.e9 (2019).
13. McGinnis, C. S., Murrow, L. M. & Gartner, Z. J. DoubletFinder: Doublet Detection in Single-Cell RNA Sequencing Data Using Artificial Nearest Neighbors. *Cell Syst* **8**, 329–337.e4 (2019).
14. Lun, A. T. L. *et al.* EmptyDrops: distinguishing cells from empty droplets in droplet-based single-cell RNA sequencing data. *Genome Biol.* **20**, 63 (2019).

Methods

Loading and visualizing bead loading in droplets

We used the 10x Chromium Controller Training Kit (PN-12024, PN-120238) to generate GEMs following manufacturer's instructions. The GEMs were carefully collected without disrupting the emulsion. After GEM formation, 10 µL of GEMs from each 10x channel was immediately loaded onto Countess Cell Counting Chamber Slides (C10228, Thermofisher) for visualization. We captured 10 bright field images under an Olympus IX70 microscope, and beads per droplet were counted based on manual inspection of images. To quantify the proportion of barcodes affected by multiple beads (barcode multiplets), we used the following equation:

$$\% \text{ multiplets} = \sum_{b=2}^{4} bn_b \,/\, \sum_{b=1}^{4} bn_b \;*\; 100$$

where b is the number of beads present in a given droplet and $n_b$is the number of droplets with b beads. Here, the expression is capped at 4 as droplets with 4+ beads could not be reliably quantified. Thus, in these instances, the value of barcodes per droplet were conservatively assigned a count of 4. For the Zheng *et. al*[2] data, we used the following abundances from previous imaging data: 15% of droplets had 0 beads; 80% of droplets had 1 bead; and 5% of droplets had 2 beads. As neither the raw data nor the quantification values have been published, these values were approximated from an examination of a plot previously reported[2].

Profiling PBMCs using 10x scATAC-seq

For 10x scATAC-seq experiments with PBMCs (PB003F, Allcells), frozen cells were quickly thawed in a 37°C water bath for about 30s and transferred to a 15 mL tube. 5 mL of pre-warmed RPMI 1640 (ATCC, 30-2001) supplemented with 10% Fetal Bovine Serum (FBS) were added to the sample drop by drop. The cells were pelleted by spinning at 300g for 5min at room temperature. The supernatant was removed and cells were washed with 1 mL PBS. The cells were then pelleted again, resuspended in 1 mL PBS, and used for 10x ATAC v1.0 protocol following manufacturer's instructions. The corresponding library was sequenced on an Illumina NextSeq 500.

Data preprocessing

Raw sequencing data was processed with Cell Ranger ATAC version 1.0.0. Reads were aligned to the hg19 reference genome available on the 10x Genomics website.

Processed 10x PBMC datasets were downloaded from https://www.10xgenomics.com/resources/datasets/ from the version 1.1 PBMC 5k scATAC-seq dataset. The requisite input files for bap included the .bam file and the high-quality barcodes file. Additional annotations from Louvain clustering and t-SNE coordinates were also downloaded for downstream visualization and analyses. For the comparison of the chip technologies (**Fig. 3g**), we again downloaded the PBMC 5k scATAC-seq datasets from the "Chromium Next GEM ATAC Demonstration."

Processing 10x scATAC-seq data with bap

In order to facilitate the processing of 10x scATAC-seq data with bap, no major substantive changes were required for the underlying barcode multiplet identification algorithm that has been previously outlined[3]. However, additional command-line options were added, including the --barcode-whitelist flag, which imports the error-corrected, quality-controlled barcodes identified as "cells" by CellRanger, enabling analysis of the filtered output from the default 10x pipeline. This functionality augments the default process in bap where abundant barcodes are identified via quantification and knee-calling in terms of total reads observed per barcode. Versions 0.5.9+ of bap facilitate full analysis and merging of barcode multiplets with 10x scATAC-seq data.

In silico mixing experiment

Using two different public PBMC 5k datasets, we sought to determine a putative false positive rate for the application of bap to 10x scATAC-seq data. Here, we denoted the PBMC-5k "Public" dataset as Channel 1 and the PBMC-5k from the NextGEM beads as Channel 2. We modified the CB tags (which contains the error-corrected barcodes) in the .bam files for each channel to ensure that each barcode for each experiment was uniquely identifiable. These modified bam files were subsequently merged. Next, the same modification to the barcodes was made, and the two high-quality barcodes files were combined into a single file. We then executed bap using the default parameters with this merged .bam and merged barcode list file. Using a single threshold determined by the knee call, we identified pairs of barcodes originating from the same or different channels as summarized in **Fig. 2c-e**. The top 500,000 barcode pairs were plotted in rank order for each of these three plots, and the same single threshold was visualized in all three panels.

Assigning bead barcodes to multiplets

The identification of multiplets follows the same strategy previously described[3]. In brief, a per-barcode pair summary statistic (modified jaccard index) is computed using the one base pair locations of Tn5 insertions. We emphasize that this statistic has been validated using an orthogonal oligonucleotide library as we have previously described[3]. From this distribution of millions of barcode pairs, we computationally infer an inflection point threshold T (similar to a "knee-call" used by CellRanger to identify true cell barcodes). To derive multiplets, we iteratively consider the barcode pairs (e.g. $b_1$and b_2) with the highest remaining overlap score and append any additional barcodes whose overlap value with either $b_1$or $b_2$exceeds T. For example, if the statistic between $b_1$and b_3 exceeds T, then b_1, b_2, and $b_3$are assigned to one multiplet. This process continues until all barcodes are assigned a multiplet that had an overlap score exceeding T. All remaining barcodes are assigned as singlets. To facilitate processing of the 10x scATAC-seq data, we modified the command line interface and internal data structures of bap, but the conceptual basis and execution is the same as previously described[3].

Classifying and quantifying complex beads

To determine multiplets driven by putative bead barcode synthesis errors, we considered all pairs of barcodes within an annotated multiplet and computed the restricted longest common subsequence (rLCS) between them. Explicitly, the rLCS is the largest consecutive number of characters that match between two strings without shifting the strings. We note the necessity of defining a distance metric (rLCS) that is distinguished from the longest common subsequence (LCS) as our metric does not allow insertions or deletions when performing the string matching. Additionally, rLCS is distinguished from the Hamming distance as the matching characters must all occur in a continuous unit (which is not enforced by Hamming).

To determine an appropriate threshold to classify multiplets as having originated from multiple beads or a single heterogeneous bead, we established a null distribution of the rLCS shown in **Fig. S3f**. To achieve this, 1,000,000 random draws of barcode pairs were determined and the rLCS was computed. We selected an rLCS threshold of 6 as pairs with an rLCS ≥6 represented less than 0.5% of the data, which was used to classify multiplets from the real data (**Fig. 3f**). To determine whether the number of fragments was similarly captured between barcodes contained in multiplets, we computed the pairwise percent difference of the log2 unique fragments ("passed_filter" in the CellRanger-ATAC .csv file). The per-multiplet average of the mean pairwise percent difference is plotted in the boxplots in **Fig. 3g**, and we used a two-sided Kolmogorov–Smirnov test to verify that the droplets containing multiple beads had a more even ratio of reads compared to multiplets driven by bead heterogeneity.

To quantify the percent of beads that had heterogeneity, the numerator was the number of multiplets identified with an rLCS ≥ 6 (from **Fig. 3f**). The denominator was the total number of barcodes analyzed while 1) still counting all barcodes in perceived bead multiplets but 2) collapsing the heterogenous barcode multiplets to only 1 barcode.

Chi-square test for cluster / multiplet

To test for association between barcode multiplets and cluster identification, we performed a chi-square test for independence. For the n Louvian clusters identified by CellRanger, we assembled a $2xn$ contingency table, tabulating barcodes into corresponding entries in the contingency table. The two rows specified whether each bead barcode was predicted to occur in a multiplet or not as identified by bap. P-values were computed using the chi-squared statistic with $n - 1$ degrees of freedom.

Evaluation of barcode multiplets with different numbers of input barcodes

To test the abundance of barcode multiplets with different numbers of considered barcodes, we executed bap with 5,000-10,000 barcodes at intervals of 1,000 barcodes (6 additional executions) in addition to the 5,205 found by CellRanger's knee call. Each barcode set was nominated based on the ranking of fragments in peaks, the same metric used by CellRanger to determine an optimal threshold. Our results (**Fig. S3b**) show that the inferred cutoff underestimates the barcode multiplets in the Public data, consistent with our imaging results. We interpret this plot to show that barcode multiplets often occur near the inflection point (consistent with these barcodes having fewer reads due to the fractionated data). However, this rate flattens when additional barcodes added do not represent multiplets but other ambient fragments that cannot be associated with a highly-observed barcode.

Enrichment for barcode multiplet pairs in the same cluster

For each barcode multiplet identified by bap, we considered all possible pairwise combinations of constitutive barcodes. For example, multiplets consisting of precisely two bead barcodes had one pair whereas multiplets consisting of four barcodes contained six barcode pairs (all combinations; choose two). For these pairs, we computed the proportion that occurred in the same Louvain cluster produced by the default CellRanger execution. A background rate was generated by performing 100 permutations of the full dataset where cluster labels were permuted.

Downsampling analyses

To evaluate the stability of the bap statistic as a function of coverage, we downsampled the dataset generated here ("This Study") at intervals of 10% and reran bap on the resulting downsampled .bam files. Here, we used the full set of high-quality barcodes determined from the CellRanger execution on the full dataset. Moreover, we determined the set of identified barcode pairs from the full dataset as a 'true positive' set of pairs to compare the downsampled results. **Fig. S3e** shows the results of this downsampling, including the 40% subsample (that corresponded to a median 10,132 fragments per barcode) that achieved >90% sensitivity in detecting the set of barcode pairs from the full data. Critically, in each of the 9 downsampled executions of bap, no barcode pairs were identified that were not present in the full dataset.

Estimation of multiplet-adjust BCR / TCR clonotype abundances

In order to estimate the number of cells contributing to each clonotype (defined by a unique BCR or TCR sequence), we downloaded the per-barcode clone identification files (BCR: vdj_v1_hs_nsclc_b_all_contig_annotations.csv; TCR: vdj_v1_hs_nsclc_t_clonotypes.csv) from the 10x CellRanger output for the public NSCLC tumor dataset. Here, each barcode is assigned a clonotype group when detected with high confidence in the CellRanger pipeline. To simulate the occurrence of barcode multiplets, we executed the following simulation procedure.

For each barcode i with a total of n barcodes in the experiment (all assigned a clonotype), we simulate a corresponding multiplet value m_i which defines the barcode multiplicity (i.e. the number of unique barcodes in the droplet) associated with the specific barcode i. This simulation was performed by drawing from the following probability distribution function:

$$P(m_i = 1) = 0.85;\ P(m_i = 2) = 0.1;\ P(m_i = 3) = 0.02;\ P(m_i = 4) = 0.02;\ P(m_i = 5) = 0.01$$

Importantly, the values defined in the probability distribution function are grounded in the empirical estimates from bap across our two datasets (see **Fig. 4d** and **Fig. 4e**) but likely represent conservative estimates assuming a similar distribution of barcode multiplets from scATAC-seq holds in this assay. In other words, $P(m_i = 1) = 0.85$ is likely overestimated and $P(m_i > 5) = 0$is underestimated. Here, we denote the set of values m_i as M(of length n). To account for k clonotypes with exactly one barcode that could only be generated from a barcode singlet, we define a new set M' such that $M' \cup K = M$ where $|K| = k$ and $\forall m_i \in K, m_i = 1$. Thus, the elements of M' represent the

barcode multiplicities for clonotypes annotated with two or more cells.

To estimate the multiplet-adjusted cell number per clonotype, we iteratively sample from the set M' until we have observed sufficient barcode numbers to explain the original clonotype abundances. More precisely, for a given clonotype j comprised of c_j barcodes (from the raw CellRanger output), we seek to compute the multiplet-adjusted number of cells c_j'. To achieve this, we sample from M' until the sum meets or exceeds c_j. c_j' then is the number of draws corresponding to the number of multiplet-aware droplets needed to explain the clonotype abundance and can be interpreted as the number of cells present in the clone under the simulation setting. Last, the new per-clonotype abundances in the library are then represented by the union of K with the set of all c_j. These multiplet-adjusted abundances were computed over 100 iterations, and the numbers reported in the main text represent the mean over these simulations. We note that an R script that achieves this approach is available in the repository noted in Code Availability.

Finally, we define the "clone false discovery rate" as the proportion of clonotypes with at least 2 cells that then becomes explained by a barcode multiplet (i.e. $c_j' = 1;\ c_j > 1$) under our simulation setting. The numbers reported in the main text represent means for each of the BCR and TCR clones over the 100 simulations.

Determination of multiplet-driven clonotypes

In scATAC-seq data, barcode multiplets were identified using our approach previously described. However, no such approach exists for scRNA-seq. Thus, to identify potential multiplets, we were required to consider potential multiplets defined only by barcode similarity, which would be reflective of synthesis errors resulting in a bead with heterogeneous barcodes (**Fig. 1a**). To determine these potential multiplets, we considered all pairs of barcodes within an annotated clonotype and computed the restricted longest common subsequence (rLCS) between them. Analysis of the distribution of pairs (**Fig. S4a**) within clonotype labels revealed was used to identify the clones shown in **Fig. 4**. When computing a permuted distribution (**Fig. S4a**), labels of clonotypes were shuffled such that random barcode pairs were considered.

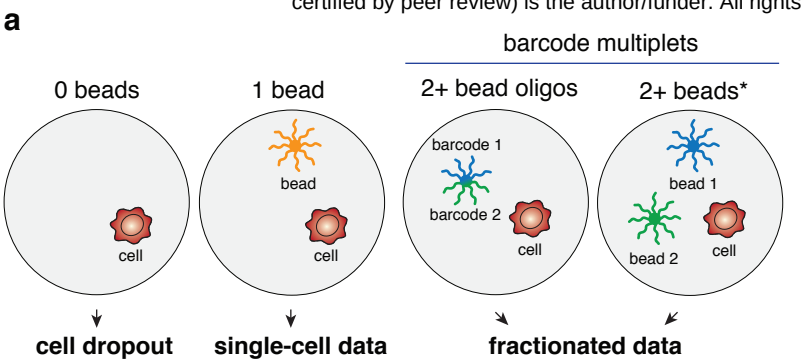

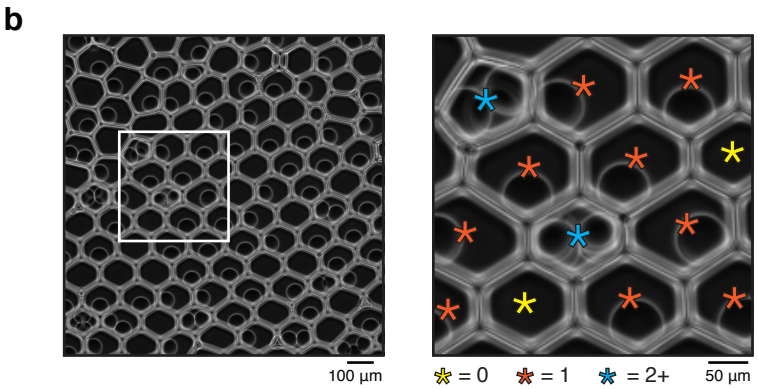

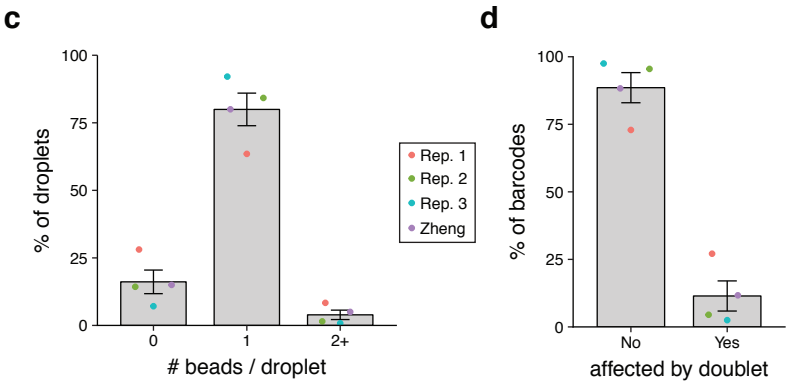

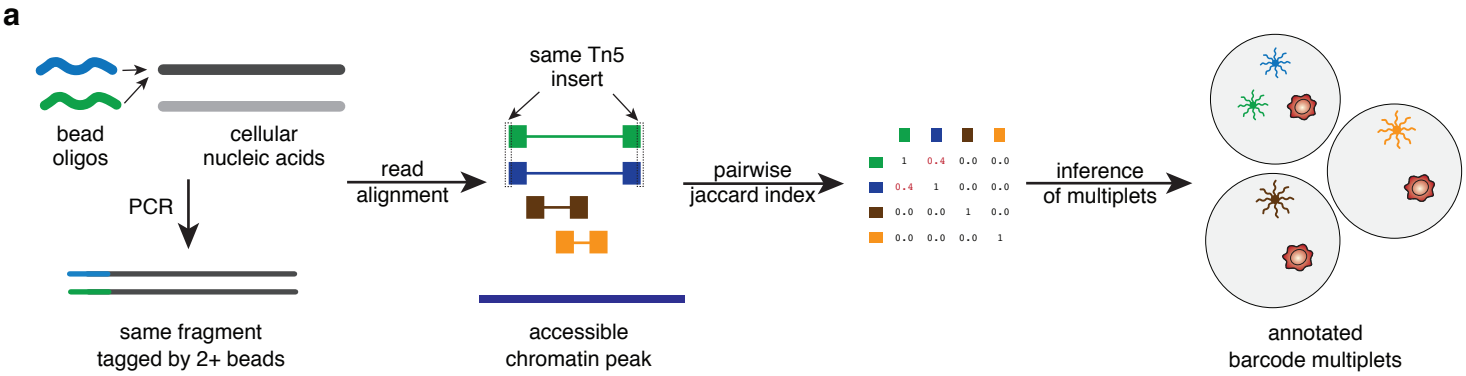

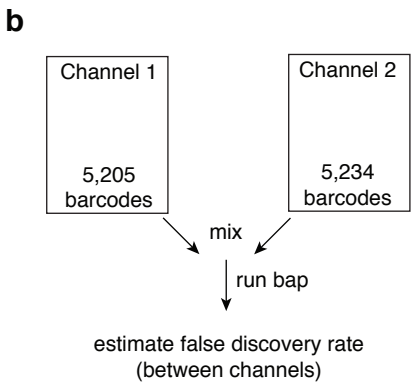

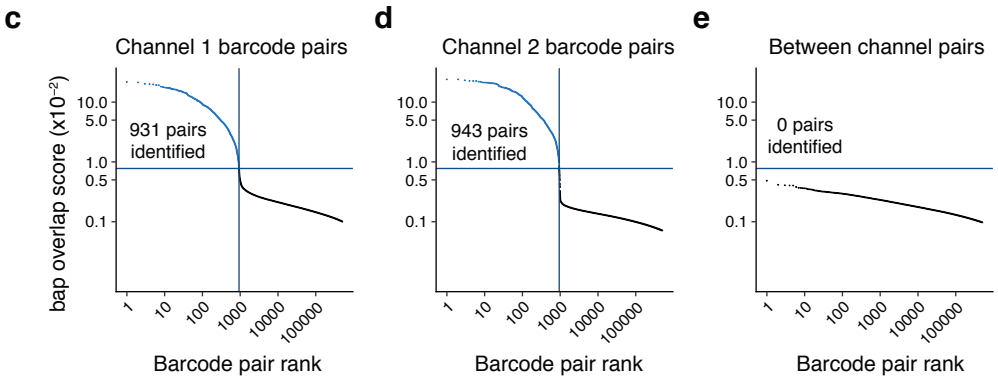

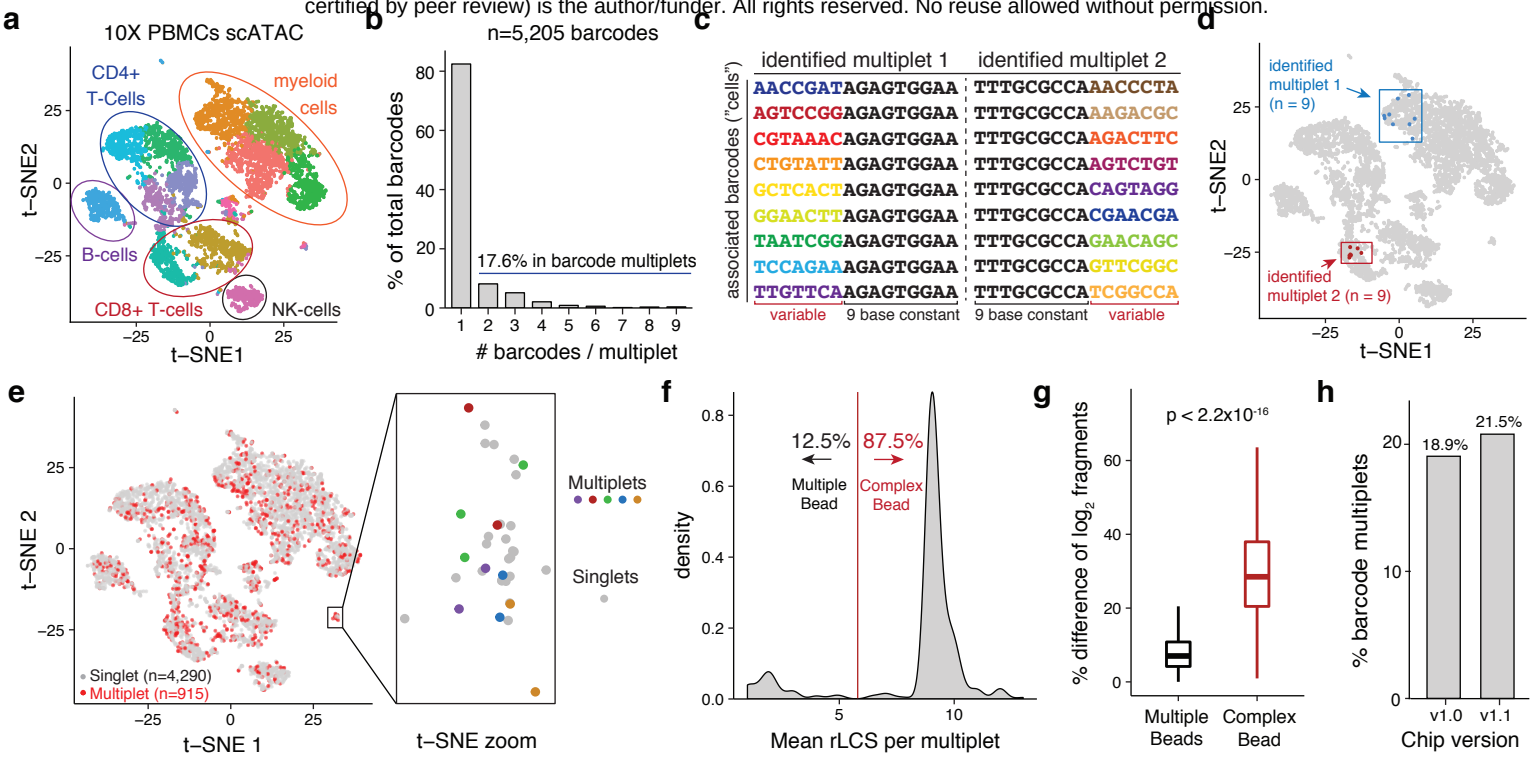

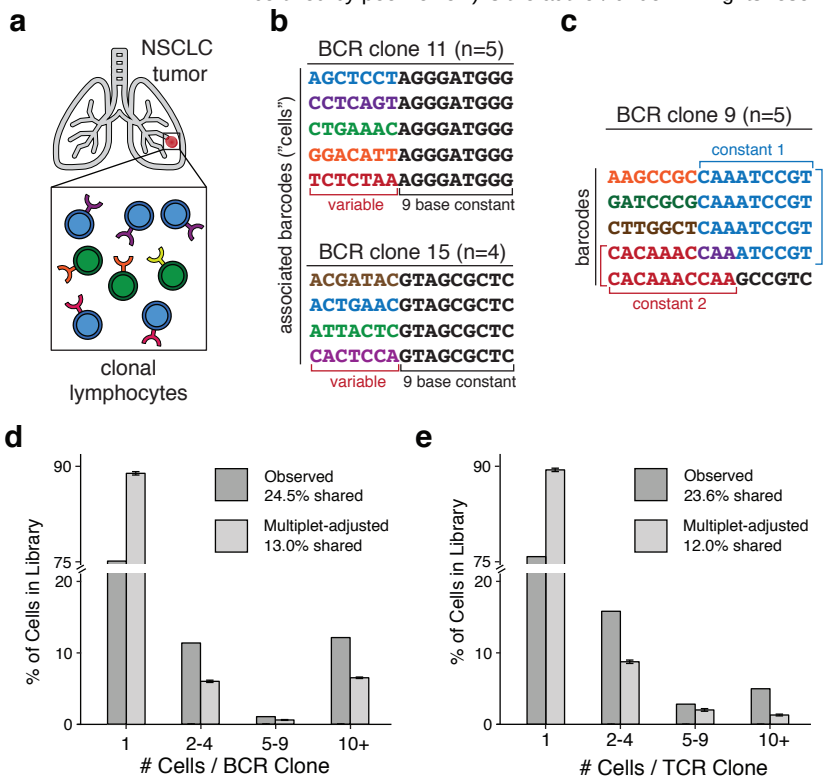

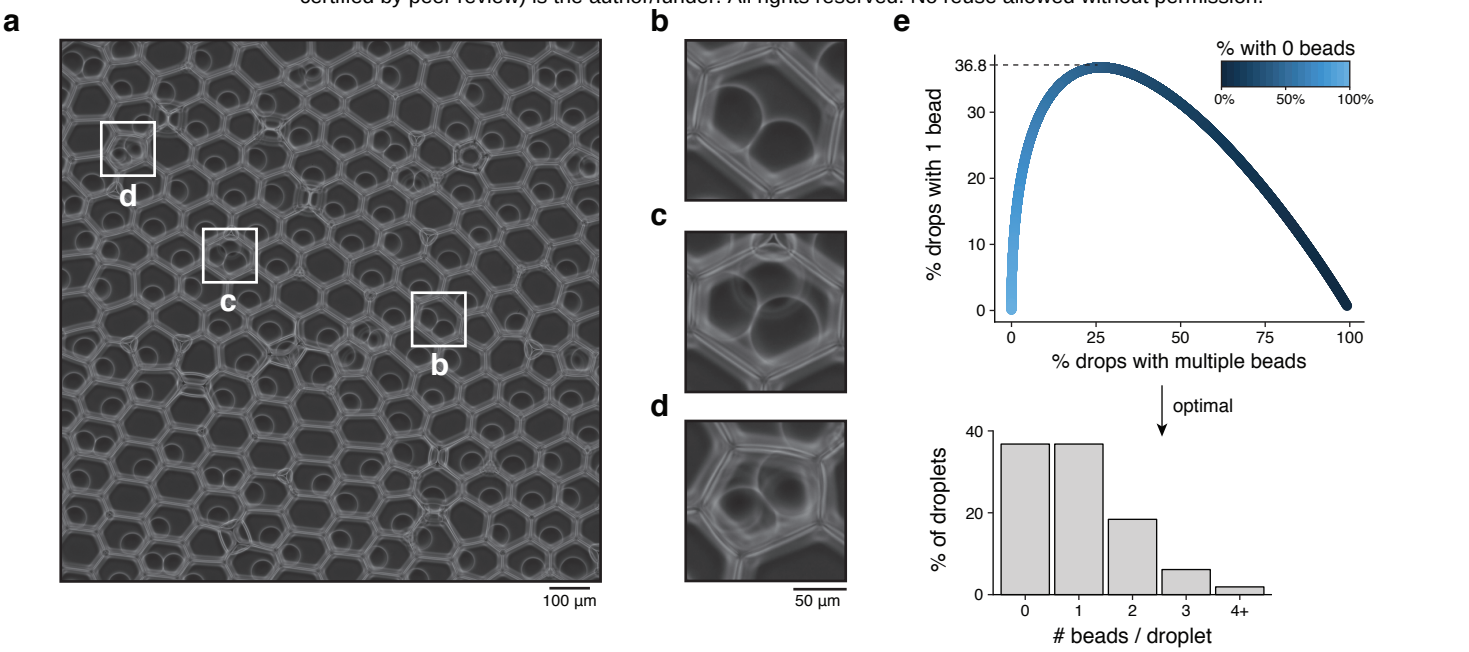

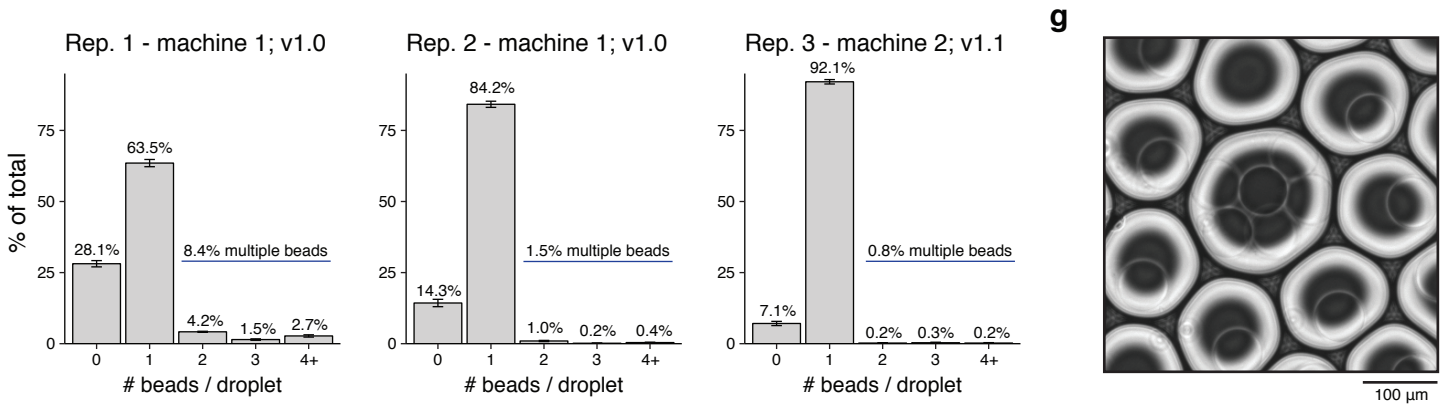

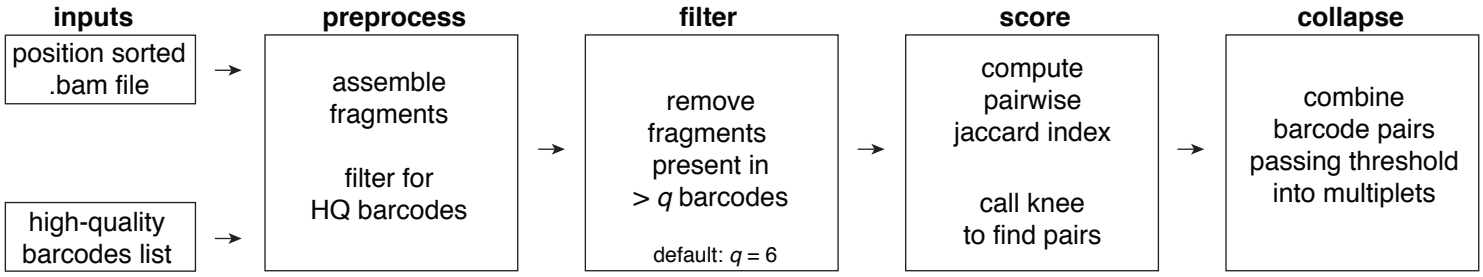

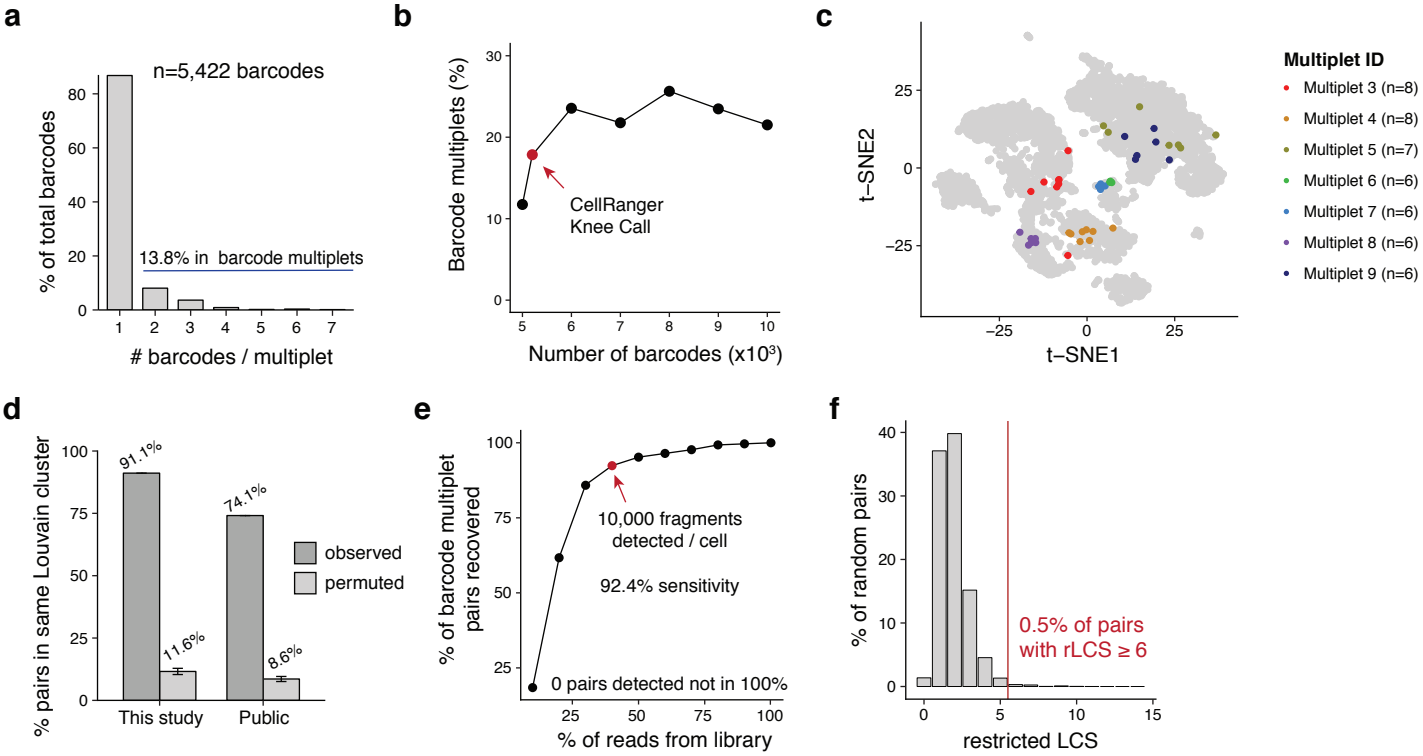

a